Nano Research
2020, 13(10): 2791–2802
ISSN 1998-0124 CN 11-5974/O4
https://doi.org/10.1007/s12274-020-2930-6

Research Article

The enhanced protective effects of salvianic acid A: A functionalized nanoparticles against ischemic stroke through increasing the permeability of the blood-brain barrier

Yaru Li[1,2], Xiaojie Zhang[1], Zhifeng Qi[3] (✉), Xueling Guo[1,2], Xiaopeng Liu[4], Wenjuan Shi[3], Yang Liu[1,2] (✉), and Libo Du[1,2] (✉)

[1] *State Key Laboratory for Structural Chemistry of Unstable and Stable Species, Center for Molecular Science, Institute of Chemistry, Chinese Academy of Sciences, Beijing 100190, China*
[2] *Graduate School, University of Chinese Academy of Sciences, Beijing 100049, China*
[3] *Cerebrovascular Diseases Research Institute, Xuanwu Hospital of Captital Medical University, Beijing 100053, China*
[4] *Department of Neurosurgery, The Second Hospital of Hebei Medical University, Shijiazhuang 050051, China*

Received: 3 May 2020 / **Revised:** 7 June 2020 / **Accepted:** 8 June 2020

ABSTRACT

Ischemic stroke is the leading cause of disability and death worldwide. Currently, the only proven treatment for ischemic stroke is restoring the cerebral blood supply. In addition, some of the tissue is damaged during the subsequent reperfusion because of the overproduction of reactive oxygen species (ROS). Furthermore, antioxidant therapies have shown promise in preclinical studies for the treatment of ischemia-reperfusion injury. However, their therapeutic efficacy has been limited because of their low bioavailability in brain. To resolve this issue, we synthesized ROS-responsive, fan-shaped dendrimer nanoparticles (NPs) and conjugated them with a blood-brain barrier (BBB)-targeting peptide, COG1410, and salvianic acid A (SA), which is an effective antioxidant in ischemic stroke. The BBB targeting peptide acts as a ligand of the nanocarrier system and penetrates the BBB through the endocytosis of the ligand receptor. The results showed that T-SA-NPs not only target and accumulate in the infarct area, they also reduce over 2 times of the infarct area and reverse the behavioral deficits in MCAO mice, which illustrates that these NPs have an effective therapeutic effect on the ischemic stroke. In addition, these NPs had no toxicity in any organs of the body. Importantly, the present study provides an alternative strategy for delivering antioxidants to the brain and achieving targeted therapy of ischemic stroke.

KEYWORDS

ischemic stroke, blood-brain barrier, salvianic acid A, COG1410, reactive oxygen species (ROS)-responsive nanocarrier, mitophagy

1 Introduction

Stroke, which is an acute cerebrovascular disease with high mortality and morbidity, ranks fifth among all causes of death. In addition, stroke is generally divided into hemorrhagic stroke and ischemic stroke [1]. Accounting for about 85% of strokes, ischemic strokes are usually a result of a cerebral infection. The main treatment for ischemic stroke is intravenous thrombolysis that is administered within 3 h after the stroke and it is considered to be the only effective treatment to restore the blood supply to the ischemic penumbra [2, 3]. However, thrombolysis may cause ischemia reperfusion injury through oxidative stress damage from reactive oxygen species (ROS) and reactive nitrogen radicals (RNS), which are produced by the excessive formation of free radicals and excitatory amino acid toxicities, respectively [4, 5]. In addition, these injuries may trigger neuronal necrosis and apoptosis, which eventually result in impaired neurological functions. Therefore, discovering an improved therapeutic intervention for ischemic stroke that doesn't come with the risk of ischemia reperfusion injury is paramount.

Considerable evidence has shown that the overproduction of ROS plays a vital role in the development of brain damage caused by ischemic stroke [6]. These ROS mediate brain damage by directly oxidizing membrane lipids [7–9], proteins and DNA [10] as well as destroying cell membranes and other functional cellular structures. In addition, these ROS activate apoptotic signaling pathways by inhibiting the function of mitochondria, which results in the selective and delayed death of neurons in the ischemic penumbra, including the hippocampal CA1 region and cortical regions [11–13]. To reduce the damage caused by ROS during ischemic stroke, a series of defense responses are activated, which increase antioxidant enzyme activity and increase the degradation of lysosomal enzymes. In addition, antioxidants play an important role in therapies for a number of diseases, including arthritis, diabetes, ischemia, atherosclerosis, and cancer, by reducing the over-production of ROS [14]. The mechanisms of action for natural compounds, such as butylphthalide, salvianolic acid B and puerarin, that are used to treat these diseases are related to their

Address correspondence to Zhifeng Qi, email_qzf@163.com; Yang Liu, yliu@iccas.ac.cn; Libo Du, dulibo@iccas.ac.cn

antioxidant activities [15–17]. Therefore, the use of antioxidants to treat ischemic stroke may be beneficial.

Salvianic acid A (SA), a long, white needle-like crystal that is easily soluble in water, is one of the antioxidants that has recieved a lot of attention. Previous study showed that SA reverses the deleterious consequences triggered by oxidative stress, such as reduced cell viability, blocked cell division cycle and decreased caspase3-dependent apoptosis [18]. In addition, SA protects against atherosclerosis by enhancing the antioxidant defense system of cells and protecting the function of mitochondria [19]. Furthermore, SA can reduce the loss of dopaminergic neurons induced by 6-hydroxydopamine (6-OHDA) in zebrafish, which supports the potential neuroprotective effect of SA [20].

Despite all of these potential benefits, there are some limitations of SA, such as it being easily oxidized, its short circulation time and its low BBB penetrance, that prevent its use in the clinic. However, recent advances in nanoscience and nanotechnology provide alternative strategies to address the limitations of SA. For example, the *in vivo* stability of antioxidants, including curcumin, coenzyme Q10 [21] and astaxanthin [22], can be significantly increased by being encapsulated in nanomaterials, such as liposomes, poly(lactic-co-glycolic acid) polymers and chitosan nanoparticles [23]. In addition, nanoparticles can increase the BBB penetrance, cirulcation time and permeability of potential therapeutics when they are used as the drug delivery system [24, 25]. For example, the antioxidant activity and BBB penetrance of quercetin and curcumin can be improved by using poly(lactide-co-glycolide) or solid lipid nanoparticles as the drug delivery carrier [26, 27]. However, these nanodrug delivery systems might result in *in vivo* oxidative damage because most of these systems are prepared through hydrophilic-hydrophobic interactions, which may induce peroxidation due to an initial sudden burst of high levels of antioxidants that are released [28]. In contrast, coupling nanocarrier delivery systems, such as polyethylene glycol, with therapeutic drugs has some merit because they improve the solubilzation of the drugs, prolong the circulation of the drugs, reduce the immunogenicity of the drugs and control the release of the drugs, which increases the safety of the drugs. Therefore, the covalent interaction between drugs and nanodrug delivery systems that have responsive characteristics provides an alternative strategy to address the limitations of SA [29].

Recent studies on nanodrug delivery systems have focused on responsive nanodrug delivery systems, the systems release their therapeutic agent under the different concentration of ROS, pH, light, glutathione (GSH) and thermal [30–36], which allow for the therapeutic agents to reach the target organs and have their release sustained. Importantly, these nanodrug delivery systems can be used to treat a number of diseases, including tumors, cancers, neurodegenerative diseases and stroke. Poly (aminoamine) (PAMAM) dendrimer derivatives have shown amazing potential as nanocarrier delivery systems because of their highly controllable molecular structures, size and biocompatibility [37, 38]. In addition, it has been shown that BBB permeability can be improved by conjugating targeting agents, such as RGDyC/PEG [39], lactoferrin [40] or triphenylphosphonium [41], with PAMAM.

Based on all these considerations, a ROS responsive nanodrug delivery system using the dendritic macromolecule, PAMAM, was designed and synthesized. After this was synthesized, SA and the targeting agent, COG1410, were conjugated with PAMAM through covalent and electrostatic interactions, respectively, resulting in the formation of BBB-targeted PAMAM (T-SA-NPs). In the current study, the *in vitro* and *in vivo* neuroprotective effects of the T-SA-NPs were evaluated in PC12 cells and mice model that simulates ischemic stroke. The T-SA-NPs nanoformulation significantly increased the accumulation of SA and decreased ROS in the brain. The use of T-SA-NPs in MCAO mice also significantly decreased neuronal damage and reversed neurobehavioral deficits cause by MCAO in mice. In addition, the *in vivo* use of these nanoparticles did not cause obvious damage or other adverse reactions in the brain or other organs. The present study provides a reliable experimental basis for delivering SA to the brain while maintaining its safe and effective administration after ischemic stroke.

2 Experimental

2.1 Preparation of nanoparticles

The PAMAM (NPs) were prepared in accordance with our previous study [42]. However, ethylenediamine was replaced by 2,2'-(propane-2,2-diylbis(sulfanediyl))diethanamine in the final step of the preparation of the NPs. NPs were covalented with SA according to the previous reported method with minor modifications [43]. Briefly, 19.8 mg of SA was dissolved in 20 mL of 0.1 M PBS (pH 6.0) and then stirred at 0 °C for 20 min. Subsequently, 23 mg of 1-(3-dimethylaminopropyl)-3-ethylcarbodiimide (EDC) was added to the mixture and then the mixture was stirred for another 1 h. Next, 0.1 g G4.0 PAMAM (40 mg) was added to the mixture. The excess EDC was removed through a dialysis membrane (molecular weight cutoff of 1,000 Da, ABI, USA). Then, the COG1410 peptide was put into the resulting mixture and stirred for 12 h. Finally, after the freeze-dried, the T-SA-NPs was obtained.

2.2 Observation of the morphology of the T-SA-NPs

The morphology of the T-SA-NPs was observed using a scanning electron microscope (Hitachi S4800, Japan). The dynamic light scattering (DLS) and zeta potential of the T-SA-NPs were measured through the use of a DLS detection system (Malvern instruments, UK) and a Zeta PALS detection system (Brookhaven Instrument, USA), respectively.

2.3 Immunofluorescence staining

Sections of paraffin-embedded brains were used for immunofluorescence staining after dewaxing according to the previous description [44]. The primary antibodies used were rabbit anti-LC3 antibody (1:200, Cell Signaling Technology), rabbit anti-β-Tublin-III antibody (1:400, Cell Signaling Technology) and rabbit anti-NeuN antibody (1:1,000, Cell Signaling Technology). The secondary antibody used was a goat anti-rabbit IgG Alexa Flour 488 at a 1:1,000 dilution (Beyotime Biotechnology co. LTD). The nucleus was stained with 4',6-diamidino-2-phenylindole (DAPI). The area of the sections that were fluorescently imaged was the ischemic penumbra, which was defined as the area between the infract and the normal tissue, and it was followed by using the fluorescence microscope.

2.4 The middle cerebral artery ischemia (MCAO) model

All animal experiments were performed according to the protocols approved by the Institute Animal Care Committee. C57BL/6 mice were split into five groups of 10 mice each. The groups were: control, MCAO, NPs, SA-NPs and T-SA-NPs. The mice were anesthetized during the operation by continuous isoflurane inhalation. In the experiment, the wire was inserted into the external carotid artery (ECA) incision position. The appropriate wire was slowly inserted from the ECA into the

internal carotid artery (ICA). The wire was made into a straight line when it was inserted into the ICA by simultaneously gently pressing down on the ECA. Then, the wire was inserted from the common carotid artery (CCA) bifurcation into the ICA along with the ECA. From here, the wire went to the anterior cerebral artery and then to the middle cerebral artery. Of note, the wire should be straight and gently inserted into the ICA. Once there is a slight resistance, the wire should be stopped [45]. Next, the extra wire is blackened and the stump is kept as long as possible to pull the wire during reperfusion. During this period, the wound was sutured and the wire was removed for reperfusion 45 min after ischemia.

2.5 2,3,5-Triphenyltetrazolium chloride staining of brain tissues

The mice were anesthetized and the brain was removed. The integrity of the brain was carefully maintained. The brain was placed on a mold in saline for sectioning, where it was sliced from rostral to caudal at 2 mm intervals. The brain slices were then placed in a 2% 2,3,5-triphenyltetrazolium chloride (TTC) solution and incubated at 37 °C for 15 min [46]. During this incubation, the brain slices were turned periodically to ensure even contact with the dye solution. The cerebral infarction area was photographed.

2.6 Hematologic examination and histology

C57BL/6 mice were intravenously injected with either the NPs, the SA-NPs or the T-SA-NPs for an *in vivo* toxicity study. Organs, including brain, heart, spleen, kidney, lung and liver, were harvested and fixed in 4% paraformaldehyde. Frozen sections were used for hematoxylin and eosin (H&E) staining. The sections with H&E staining were observed by using inverted fluorescence microscope.

2.7 The biodistribution of NPs and T-NPs in the MCAO model in mice

C57BL/6 mice and MCAO C57BL/6 mice were administered NPs-Texas Red or T-NPs-Texas Red by intravenous injection or tail vein injection, respectively. After 6 h, the brain, heart, spleen, kidney, lung and liver of the animals were harvested and imaged with a Caliper IVIS Lumina II (Spectrum CT).

2.8 Statistical analysis

All data presented are expressed as the means ± standard deviation (SD) and analyzed using SPSS 20.0 software. All experiments were statistically analyzed by one-way ANOVA. The data were regarded as statistically significant at $^{*}P < 0.05$ or highly significant at $^{**}P < 0.01$.

3 Results and discussion

3.1 Physicochemical characterization

Of the responsive nanodrug delivery systems, we used the ROS responsive nanodrug delivery system because of the higher concentrations of ROS in neurodegenerative diseases. In the present study, a ROS responsive nanodrug delivery system based on the PAMAM (T-SA-NPs) was synthesized. T-SA-NPs were prepared as shown in Fig. 1(a). First, SA was

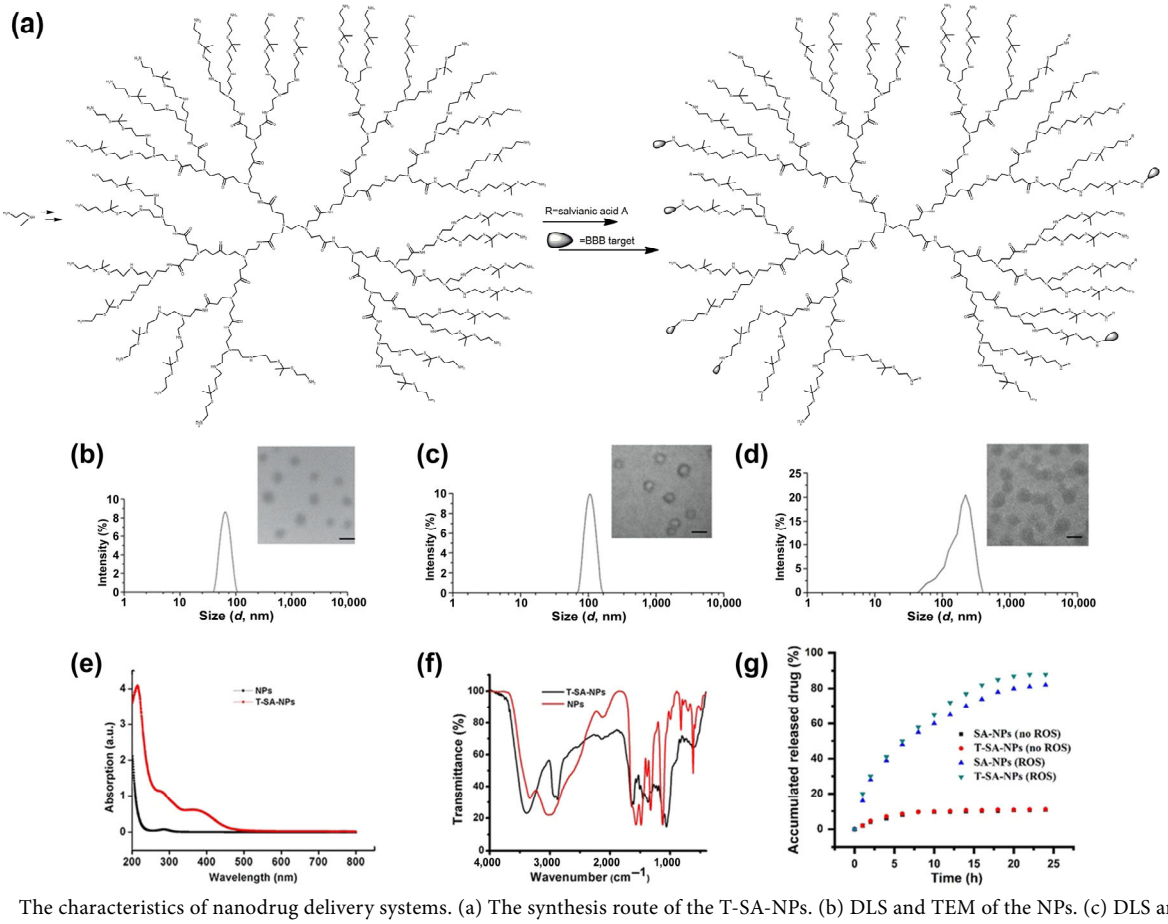

Figure 1 The characteristics of nanodrug delivery systems. (a) The synthesis route of the T-SA-NPs. (b) DLS and TEM of the NPs. (c) DLS and TEM of the SA-NPs. (d) The DLS and TEM of the T-SA-NPs. (e) UV–Vis spectra of the NPs and the T-SA-NPs. (f) FTIR spectra of the NPs and the T-SA-NPs. (g) The release plot of the SA-NPs and the T-SA-NPs under condition of reactive oxygen species (scale bar: 100 nm).

conjugated with generated 4.0 ROS-responsive PAMAM through an esterification reaction to prepare SA functionalized ROS-responsive PAMAM (SA-NPs). Then, SA-NPs were conjugated with blood-brain barrier (BBB) targeting agents (COG1410) by electrostatic interactions to prepare the targeting nanodrug delivery system (T-SA-NPs), which was then characterized by transmission electron microscopy (TEM), Fourier-transform infrared spectroscopy (FTIR), DLS and zeta potential. The TEM and DLS results demonstrated that both the SA-NPs and the T-SA-NPs possessed typical structures with spherical and uniform size as well as uniform distribution and good polydispersity (Figs. 1(b) and 1(d)). In addition, the T-SA-NPs were characterized by FTIR (Fig. 1(f)) and ultraviolet–visible (UV–Vis) absorption spectroscopy (Fig. 1(e)). As shown in Fig. 1(f), the peaks at 1,400–1,600 and 2,876 cm^{-1} were ascribed to the stretching vibration of the benzene ring and C–H (CH_3). As shown in Fig. 1(e), there is a characteristic absorption peak at 280 nm in the UV–Vis spectrum of the T-SA-NPs. Based on these results, SA has been functionalized on the surface of PAMAM. In addition, the loading efficiency of SA on the SA-NPs was 13.6% as determined by UV–Vis spectroscopy.

Next, a release study of SA was employed simulated ROS (Feton reaction). As shown in Fig. 1(g), the SA was released from SA-NPs and T-SA-NPs within 1 h in the ROS condition whereas there was nearly no SA release without the presence of ROS, which indicates that SA-NPs can specifically release SA in certain conditions.

3.2 Safety of the nanoparticles and their enhanced cellular uptake *in vitro*

To determine the safety of the nanoparticles, an methyl thiazolyl tetrazolium (MTT) assay was used to evaluate their activity in cells. A variety of PAMAM with concentrations ranging from 0 to 800 μg/mL were added to PC12 cells and the viability of PC12 cells was determined after 12 and 24 h (Fig. 2(b)). The results showed that the nanoparticles were safety to PC12 cells and without biotoxicity in 12 and 24 h.

Next, in order to detect the therapeutic strategies of nanoparticles, the experiment was divided into six groups including control, OGDR, OGDR+NPs, OGDR+SA, OGDR+ SA-NP and OGDR+T-SA-NPs. Except control group, the other five groups processed 4 h oxygen glucose deprivation (OGD) and 24 h reoxygenation that was named OGDR (Fig. 2(a)). The nanodrug delivery systems were added to two different types of cells, PC12 and HT22, after 24 h to determine their activity in cells. The viability of cells treated with NPs, SA-NPs or T-SA-NPs was significantly increased compared to the cells that underwent OGDR without treatment. In addition, the viability of cells treated with T-SA-NPs was significantly increased compared with cells treated with SA-NPs (Fig. 2(c)).

In order to obtain a fluorescently-labeled nanodrug delivery system, Texas Red was conjugated with the T-NPs (T-NPs-Texas red), which allowed for the evaluation of the cellular-uptake of the T-NPs-Texas red. PC12 cells were incubated with T-NPs-Texas red for 2, 4, 6 and 12 h and then the cells were washed and fixed. The results demonstrated that the fluorescence intensity in cells increased with the length of incubation time. The enlarged merged images show that after entering the cells, the nanoparticles increasingly accumulated in lysosomes with time, which potentially indicates that the nanoparticles enter cells through the lysosomal pathway (Fig. 2(d)).

Then, the endocytosis of COG1410-mediated nanoparticles on the monolayer capillary endothelial cell was studied as an *in vitro* model for nanoparticles to penetrate the BBB. The

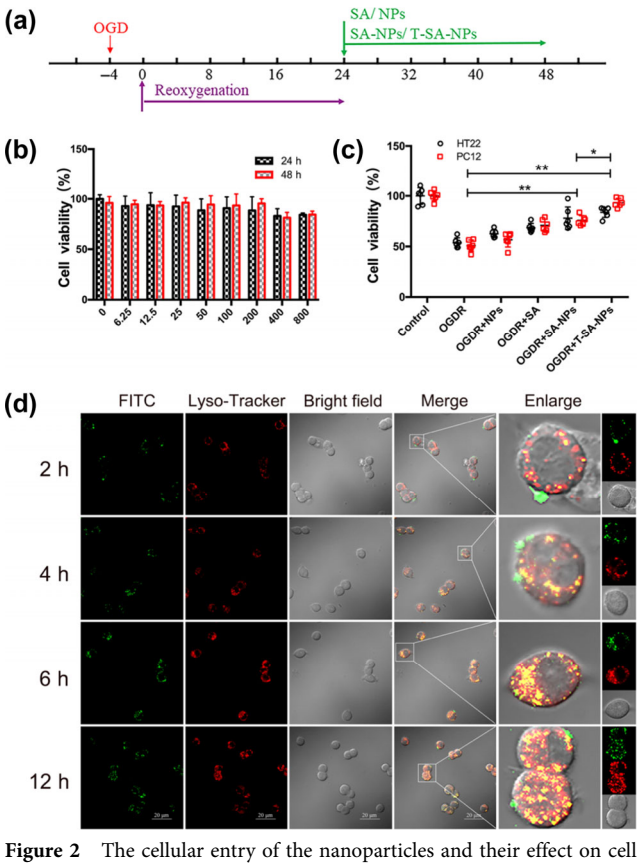

Figure 2 The cellular entry of the nanoparticles and their effect on cell viability. (a) Experiment schedule of the OGDR cell model and the administration of nanoparticles formulations. (b) The viability of PC12 cells was detected by MTT. The concentrations of the nanoparticles used were 0, 6.25, 12.5, 25, 50, 100, 200, 400, and 800 μg/mL. The nanoparticles were co-incubated with PC12 cells or HT22 cells for 24 and 48 h. The viability of the PC12 cells was detected by MTT. Black represents 24 h. Red represents 48 h. The data is presented as mean ± SD (n = 6); *p < 0.05; **p < 0.01. (c) The protective effect of the nanoparticles on cells after OGDR. The experiment was performed with two kinds of cells, HT22 (mouse hippocampal neuronal) cells and PC12 (rat pheochromocytoma parent) cells. Black represents HT22 cells and red represents PC12 cells. (d) Nanoparticles entered into cells. FITC-nanoparticles were co-cultured with PC12 cells and then co-localized with lysosomes after 2, 4, 6 and 12 h. Green represents the nanoparticles attached to FITC. Red represents the lysosome in the cell. The merge is the co-localization of the nanoparticles with the lysosome. Scale bar = 20 μm.

monolayer of endothelial cells grown on transwell inserts was incubated with medium, Texas red, NPs-Texas red or T-NPs-Texas red, and the supermatant and the basolateral were detected by a microplate reader (Fig. S1 in the Electronic Supplementary Material (ESM)). The results showed that the fluorescence signal after 4 h T-NPs-Texas red incubation was 2.2 times higher in the basolateral than incubation with NPs-Texas red (Fig. S1 in the ESM), which suggesting a specific interaction between the T-NPs-Texas red and bEnd.3 cells.

3.3 Antioxidative activities of the T-SA-NPs *in vitro*

The overproduction of ROS is closely associated with aging [47] as well as with the pathology of many diseases, including cancer [48], inflammatory diseases [49] and degenerative diseases (e.g., Alzheimer's disease (AD) [50], Parkinson disease (PD) [51] and stroke [52]). Therefore, the removal of intracellular ROS is potentially an important strategy in disease therapies.

Superoxide anions are the first ROS generated after oxygen enters living cells, which are then converted to ROS. Therefore,

the detection of both superoxide anions and ROS is important for the evaluation of the effects of antioxidants. To investigate the antioxidant activities of the T-SA-NPs, ROS in cells and mitochondria was measured using DCFH-DA (a ROS fluorescence probe) and Mito-SOX (a mitochondrial superoxide anion fluorescence probe), respectively. After OGDR- simulated ischemic stroke, which can induce the production of ROS, the level of ROS in cells and in mitochondria were increased compared with the control group. However, the ROS levels in cells and in mitochondria treated with NPs, SA-NPs or T-SA-NPs were significantly decreased compared with OGDR. In addtion, the ROS levels in the T-SA-NPs-treated group significantly decreased compared with the SA-NPs-treated and NPs-treated groups, which demonstrate that the T-SA-NPs remove ROS from cells more effectively (Figs. 3(b) and 3(d)). As shown in Figs. 3(a) and 3(c), the apoptosis rates in both the SA-NPs-treated and the T-SA-NPs-treated groups were significantly reduced compared with the OGDR group. In addition, the T-SA-NPs-treated group increased the survival rate of cells and exhibited an increased protective effect compared with the SA-NPs-treated group.

The molecular mechanism of the protective effect of the T-SA-NPs was investigated by western blot, which detected the expression of proteins related to mitochondria-mediated apoptosis, including Bax, Bcl-2, caspase3 and pro-caspase3. As shown in Fig. 3(e), the ratio of Bax/Bcl-2 was increased in the OGDR group compared with control. However, pretreatment of cells with SA-NPs or T-SA-NPs up-reguated the levels of Bcl-2 and decreased the ratios of Bax/Bcl-2 and pro-caspase3/caspase3 (Fig. 3(e)). Furthermore, the T-SA-NPs showed a more significant protective effect after the OGDR than the same concentration of SA-NPs did. As shown in Fig. 3, the treatement with T-SA-NPs induced the up-regulation of Bcl-2 and the down-regulation of Bax, which indicates the inhibition of Bax/Bcl-2-binding or Bax/Bax-binding permeability transition pores (PTP). PTP that promotes the formation of apoptosome based on apaf-2 and pro-caspase-9 inhibits the release of cytochrome C. And activated caspase-9 did not proteolyze Pro-caspase3, which further inhibited PARP cleavage, thereby promoting cell survival.

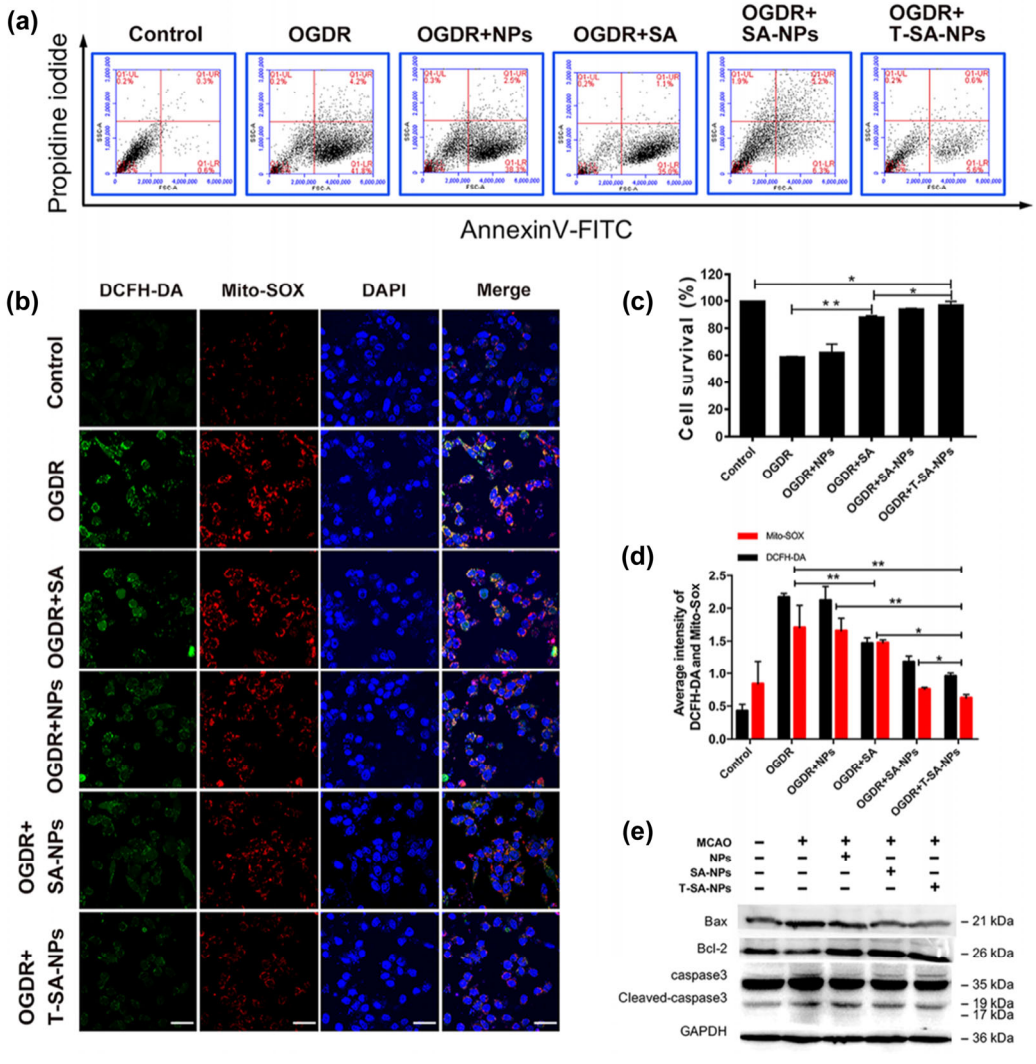

Figure 3 The level of intracellular ROS and cell apoptosis after injection of NPs, SA-NPs or T-SA-NPs. PC12 cells were first subjected to OGD for 4 h and then reoxygenated for 24 h. At the same time, different nanoparticles were added to measure the content of ROS and mitochondrial superoxide by immunofluorescence. (a) Analytical images of cell apoptosis by flow cytometry after OGDR treatment. (b) DCFH-DA was used for the detection of ROS in cells and Mito-Sox was used to detect mitochondrial superoxide. Scale bar = 20 μm. (c) The apoptosis of each group was analyzed by one-way ANOVA. Data are presented as the mean ± SD (n = 3); *p < 0.05; **p < 0.01. (d) The DCFH-DA and Mito-Sox of each group were analyzed by one-way ANOVA. Data are presented as the mean ± SD (n = 3); *p < 0.05; **p < 0.01. (e) Western blot analysis of Bax, Bcl-2 and caspase3 in mice treated with NPs, SA-NPs or T-SA-NPs as well as untreated mice. The statistics of each group were analyzed by one-way ANOVA. Data are presented as the mean ± SD (n = 3); *p < 0.05; **p < 0.01.

3.4 T-SA-NPs protect neurons by inducing mitochondrial autophagy

Mitochondria are the main organelle where cells produce adenosine triphosphate (ATP) [53]. During the oxidative process of mitochondria, the energy generated by the electrochemical potential is stored in the inner membrane of the mitochondria, which results in an asymmetric distribution of proton plasma concentrations across the inner membrane of the mitochondria and this forms mitochondrial membrane electricity (MMP) [54]. The MMP, which plays a coupling role in the process of mitochondrial oxidative phosphorylation, is a prerequisite for maintaining the mitochondria function as energy factories by producing ATP [55]. The stability of the MMP is conducive to maintaining the natural physiological functions of cells. Recent studies have found that the MMP of cells start to decline prior to pathological changes in the early stage of apoptosis [56]. Therefore, a change in the MMP in PC12 cells could be an indicator of mitochondira dysfunction. Thus, the MMP of PC12 cells was measured by a JC-1 fluorescence probe and the results showed that both OGDR and OGDR+NPs decreased the MMP of cells and induced cell damage. However, the T-SA-NPs repaired the MMP of PC12 cells that were damaged by OGDR (Figs. 4(a)–4(c)).

According to previous studies [57], the change of MMP or mitochondrial membrane opening generally induce mitochondrial autophagy (mitophagy), which plays an important role in reducing mitochondrial DNA mutations that are caused by aging. Therefore, we speculated that mitophagy may be closely associated with the MMP change. The expression of LC3, an important marker of autophagy that is responsible for the formation of autophagosomes, was determined in PC12 that underwent OGDR (Fig. 4(d)). Treatment of these cells with either the SA-NPs or the T-SA-NPs increased the expression of LC3 II in comparison with the OGDR, OGDR+SA and OGDR+NPs groups. In addition, the expression of Pink1, Parkin and Beclin1, which are involved in mitophagy, was significantly higher in the T-SA-NPs treated group than that

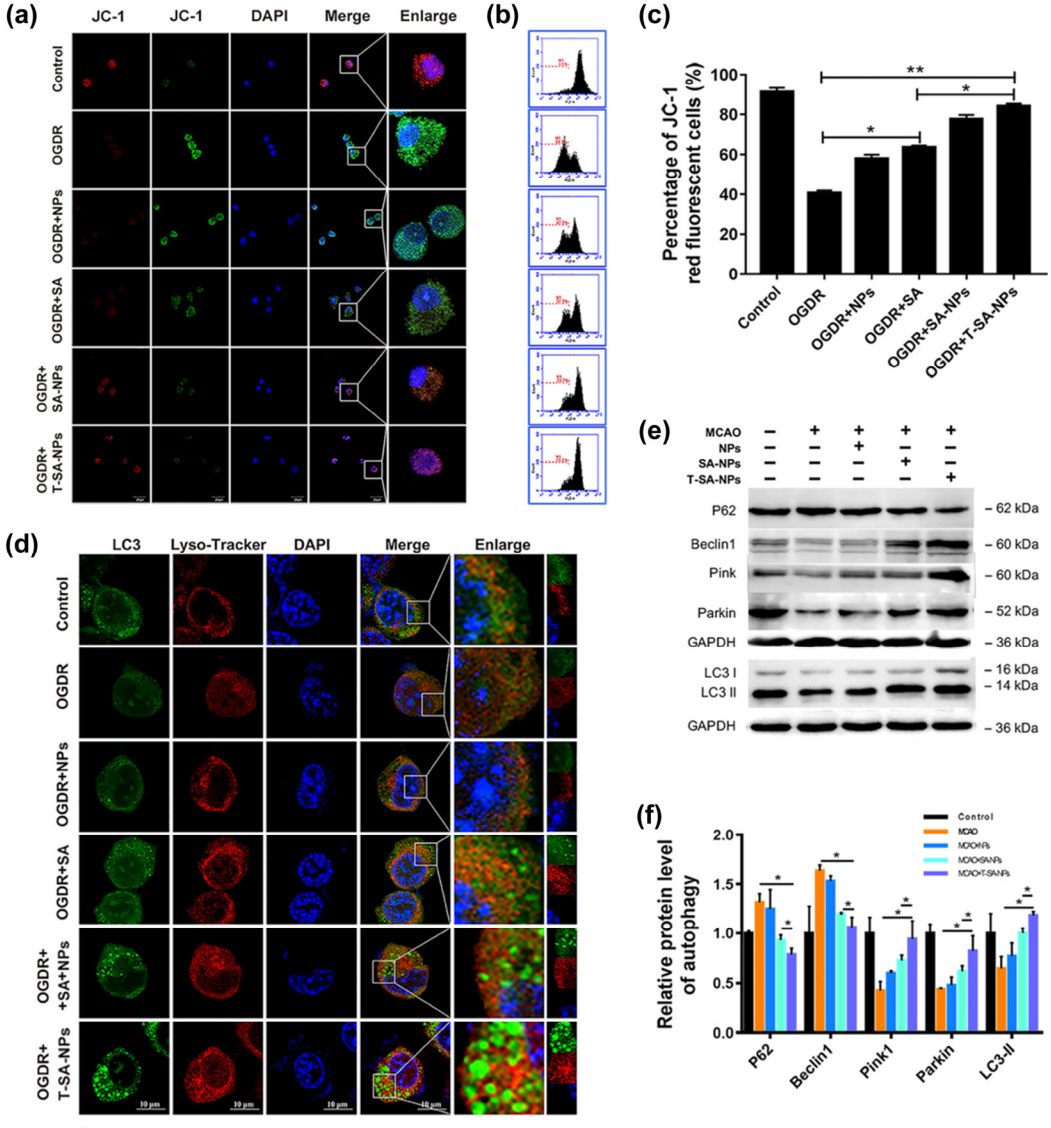

Figure 4 Detection of mitochondrial membrane potential and autophagy in cells. (a) JC-1 was used to detect mitochondrial membrane potential by immunofluorescence. When the mitochondrial membrane potential increases, it appears red and when it decreases the green will be brighter. (b) After the cells were subjected to OGDR treatment, different nanoparticles were added and then the cells were stained with JC-1, which was detected by flow cytometry. (c) Statistical analysis of the flow cytometry results. Data are presented as the mean ± SD (n = 3); *p < 0.05; **p < 0.01. (d) Detection of mitochondrial autophagy. LC3 is a marker of autophagy. Lyso-Tracker is a marker of lysosomes. The degree of autophagy occurs after colocalization of LC3 with lysosomes. (e) Western blot of autophagy proteins, including LC3, P62, Beclin1, Pink1 and Parkin, in the penumbra area after treatment with NPs, SA-NPs or T-SA-NPs. (f) Western blot analysis was performed by one-way ANOVA. Data are presented as the mean ± SD (n = 3); *p < 0.05; **p < 0.01.

in the other groups (Figs. 4(e) and 4(f)). Furthermore, treatment with the T-SA-NPs cleared the damaged mitochondria through mitophagy resulting in the decrease of oxidative stress.

3.5 The biodistribution and brain targeting of nanoparticles around the penumbra field *in vivo*

To investigate the targeting effect and biodistribution of the nanodrug delivery systems *in vivo*, the biodistribution of the NPs-Texas Red and the T-NPs-Texas Red were assessed in naïve mice and mice that underwent MCAO. Mice were euthanized and perfused with saline for *ex-vivo* imaging 6 h after the administration of the NPs-Texas Red and T-NPs-Texas Red. As shown in Fig. 5(a), the Texas Red-conjugated nanoparticles in mice with or without MCAO accumulated in the brains and livers. Interestingly, the fluorescence intensity in the brains of the control group that were administered T-NPs-Texas Red was much higher than in the brains of control mice that were administered NPs-Texas Red, which indicates that the targeting peptides were more conducive to the drugs crossing the BBB. In addition, the fluorescence intensities in the brains of MCAO mice administered T-NPs-Texas Red or NPs-Texas Red were much higher compared with those of the control mice and indicates that the drug delivery systems targeted the lesions more easily as a result of ischemic stroke. Furthermore, the fluorescence intensities in the brains of T-NPs-Texas Red-treated MCAO mice were significantly higher than in the brains of NPs-Texas Red-treated MCAO mice, which indicates the better targeting of T-SA-NPs to the injured brain (Fig. 5(b)).

In order to fully perform the therapeutic effects of SA, the nanoparticles must be transported to the penumbra area of cerebral ischemia, which is the main part in need of rescue

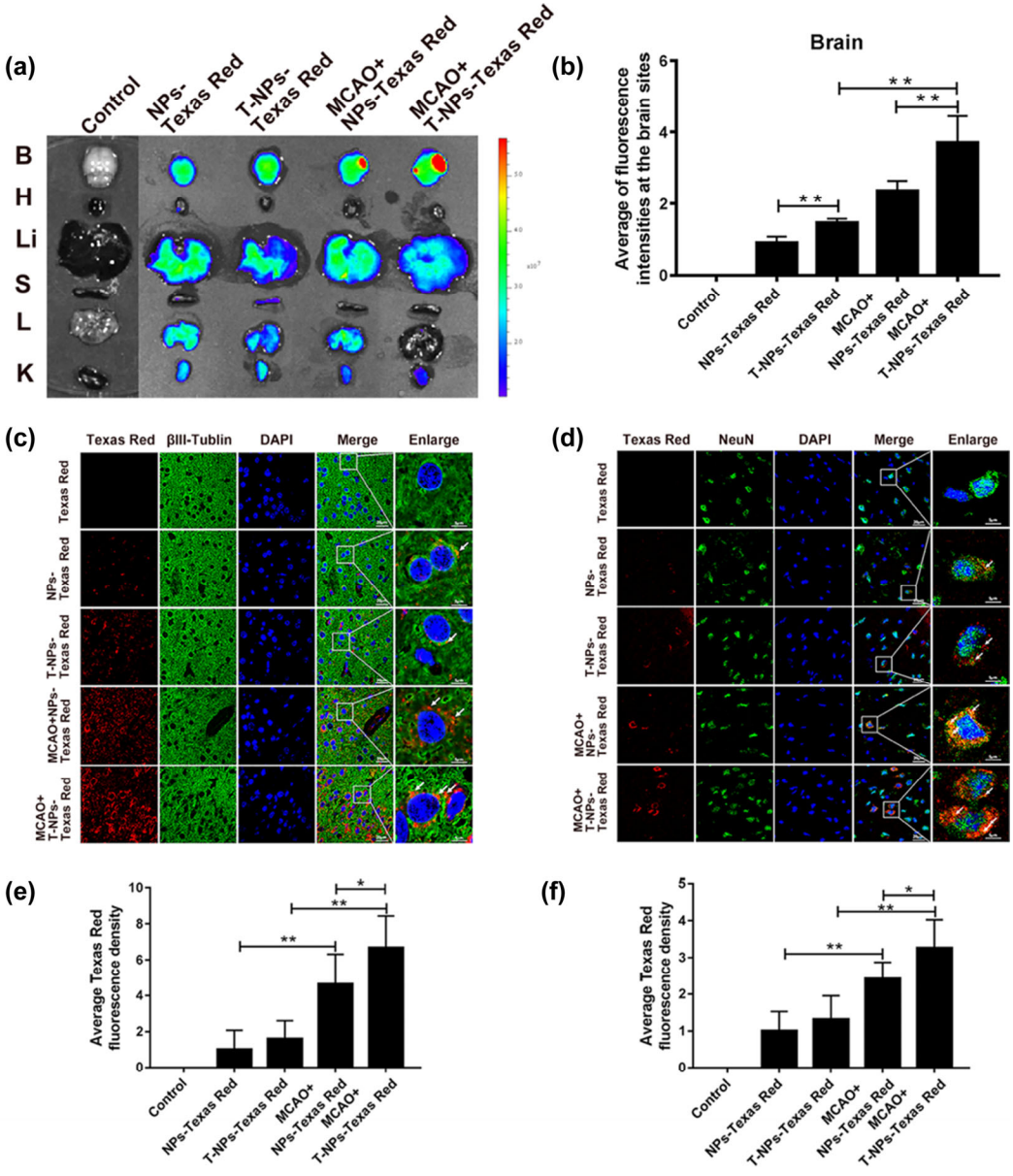

Figure 5 T-NPs targeted the brain *in vivo*. (a) Fluorescence images of the brain and other main organs of mice 6 h after injecting nanoparticles, such as Texas Red, NPs-Texas Red or T-NPs-Texas Red via the tail vein. (b) After the intravenous injection, the average fluorescence intensity of the mouse brains were quantified. Data are presented as mean ± SD (n = 3); $^{**}p < 0.01$. (c)–(f) Typical confocal images of β-III Tublin (c) and NeuN (e) dispose of Texas Red, NPs-Texas Red and T-NPs-Texas Red 6 h post-injection. The neurons were identified by immunostaining (green) for β-III Tublin (c) and NeuN (green) (d) in the penumbra area. The nuclei were stained with DAPI (blue). The presence of nanocarriers (red) in neuronal cells is indicated in the enlarged rightmost column. Scale bar = 20 μm. The Texas Red fluorescence densities are quantified in (d) for β-III Tublin and (f) for NeuN using Image J. Data are presented as mean ± SD (n = 3); $^{*}p < 0.05$; $^{**}p < 0.01$.

after cerebral ischemia. Laser confocal microscopy analysis found that both NPs-Texas Red and T-NPs-Texas penetrated the penumbra while Texas Red alone did not. In addition, the COG1410-modified targeting nanoparticles showed prominently stronger aggregation compared with other groups (Figs. 5(c) and 5(d)). Furthermore, immunofluorescence staining of βIII-tubulin also revealed that the nanoparticles colocalized with neurons. Therefore, both the NPs-Texas Red and the T-NPs-Texas Red co-localize inside or near the neuron for 6 h after tail vein injection, which confirms that the nanoparticles can enter neurons *in vivo* (Figs. 5(e) and 5(f)).

3.6 T-SA-NPs administration decreases behavioral impairment in mice after ischemic stroke

To build upon the *in vitro* protective effect of T-SA-NPs after OGDR, the therapeutic effect of T-SA-NPs was evaluated in ischemic brains by TTC staining, immunohistochemical analysis and behavioral tests 24 h after injury (Fig. 6(b)). As shown in Figs. 6(a) and 6(e), there were no infract zones or behavior impairment in the control group in comparison to the severely damaged infract areas and behavioral impairments seen in the MCAO group. Importantly, there was a significant decrease in the brain infected areas in the SA-NPs-treated and T-SA-NPs-treated groups compared with the untreated MCAO group (Fig. 6(c)). In addition, the average residence time of T-SA-NPs-treated MCAO mice on the balance beam was increased compared with MCAO mice and SA-NPs-treated MCAO mice (Figs. 6(f) and 6(g)), which indicates that the nanoparticles conjugated with COG1410 can reduce behavioral impairments and infarct size as a result of ischemic stroke.

Furthermore, immunostaining in the brain showed that there was a significant recovery of neurons after treatment with SA-NPs or T-SA-NPs. The T-SA-NPs-treated group showed more recovery than the SA-NPs-treated group, which indicates that the T-SA-NPs exhibit a higher targeting effect (Fig. 6(d)). Taken together, these results demonstrate that the delivery of SA by COG1410-modified nanoparticles can significantly improve the behavioral outcomes in MCAO mice. Furthermore, COG1410-modified nanoparticles are more efficacious than the SA-NPs or non-targeted nanoparticles in treating ischemic stroke in mice.

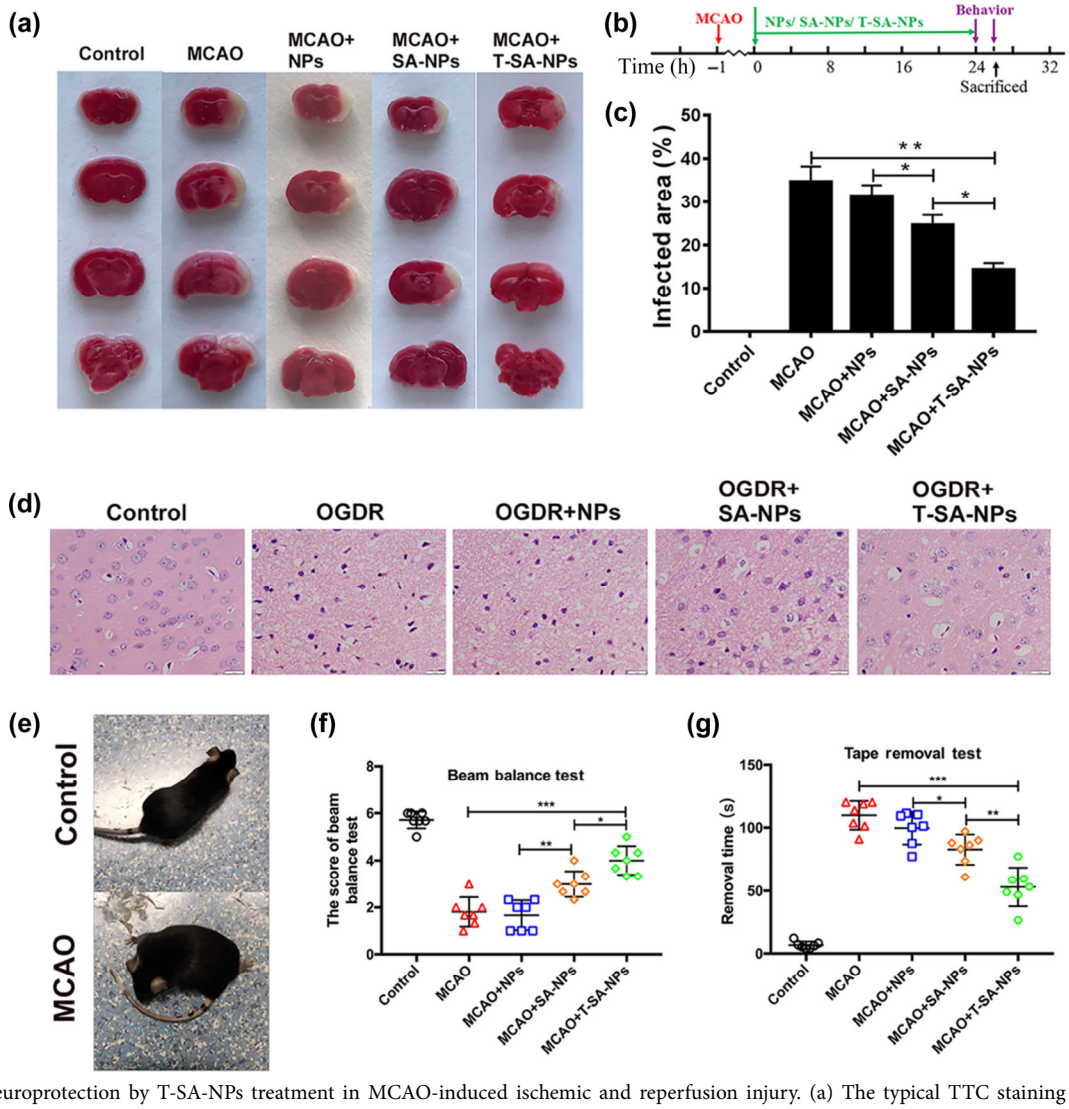

Figure 6 Neuroprotection by T-SA-NPs treatment in MCAO-induced ischemic and reperfusion injury. (a) The typical TTC staining of the control group, MCAO group, NPs group, SA-NPs group and T-SA-NPs group. The red is the natural area region and the white shows the infarct region. (b) The experiment schedule of the MCAO model and the administration of the nanoparticles formulations. (c) Treatment with T-SA-NPs significantly reduced ischemic lesion size. Data are presented as the mean ± SD (n = 5); *p < 0.05; **p < 0.01. (d) Histological analysis of neuronal cells. Intact cells indicate normal tissue. Karyopyknosis indicates cell apoptosis and necrosis. Scale bar: 20 μm. (e) Behavior normal mice and MCAO mice are different. (f) and (g) Behavioral manifestation of MCAO in mice in the beam balance test (f) and tape removal test (g) after NPs, SA-NPs or T-SA-NPs therapy. Mice in the control group were injected with saline instead. Data are expressed as mean ± SD (n = 7). Statistical analysis used was one-way ANOVA test.

3.7 T-SA-NPs treatment decreases oxidative stress in the penumbra region in the MCAO model

After ischemic stroke, microglial activation results in an upregulation of inflammatory mediators and migrated from the peripheral lesions to the lesions. Here, a multitude of detrimental molecules, including free radicals, glutamate, chemokines and cytokines, are released by activated glial cells and infiltrating leukocytes in the lesion. These inflammatory molecules eventually lead to the destruction of the BBB, encephaledema and the exacerbation of neuronal death [58]. Therefore, to determine whether SA-NPs or T-SA-NPs administration reduces cacoethic inflammation in the brain, the mRNA levels of inflammatory factors, including TNF-α, IL-1β and IL-6, in the penumbra were measured (Figs. 7(a)–7(c)). The results demonstrated that SA-NPs or T-SA-NPs administration reduced the inflammatory damage associated with ischemic stroke as previous studies have shown that the process of stroke is accompanied with inflammation, which induces cell apoptosis. Figures 7(a)–7(c) show that these nanodrug delivery systems can inhibit stroke-associated inflammation as evidenced by the decrease in IL-1β, IL-6 and TNF-α.

One of the mechanisms of neurotoxicity after ischemic stroke may be the sudden influx of oxygen during reperfusion, which may cause damage as a result of oxidative stress and lead to neuronal death. To test this hypothesis, the oxidative stress levels in the hippocampi in MCAO mice after treatment with T-SA-NPs were examined. The results show that the level of SOD (superoxide dismutase) in the hippocampi from MCAO mice were significantly decreased after T-SA-NPs treatment (Fig. 7(d)). Similar results were obtained by measuring other indicators of oxidative stress, including malondialdehyde (MDA; Fig. 7(e)) and GSH (Fig. 7(f)). As shown in Fig. 5(a), the nanodrug delivery system accumulated in the brain because of the targeting effects on BBB. Once in the brain, the nanodrug delivery system penetrates the infarction area through the BBB where the antioxidants are released from the nanodrug carriers under the condition of ROS overproduction. Here, the antioxidants decrease ROS where the overproduction of ROS might aggravate the impairment of mitochondrial function that is essential for cell function and survial, particularly in neurons [59–61].

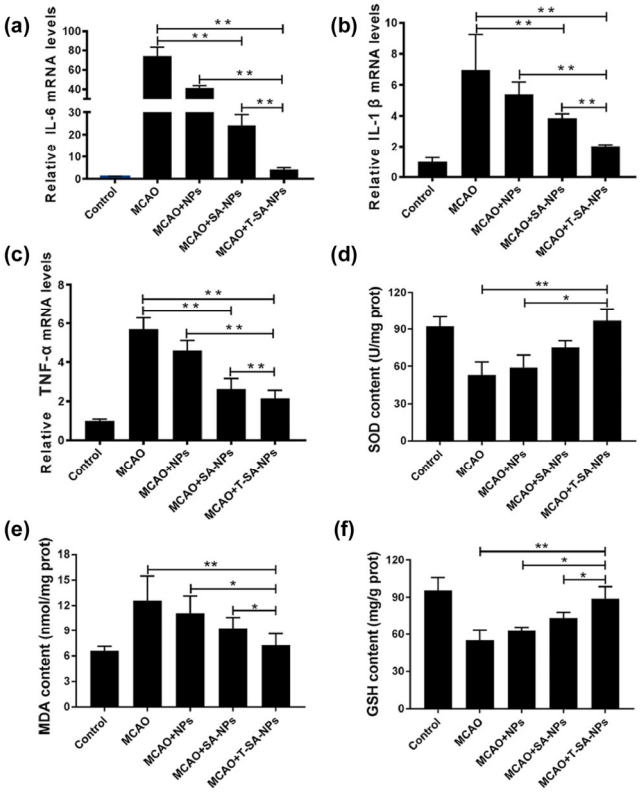

Figure 7 The anti-inflammatory and antioxidant effects of the nanoparticles. (a)–(c) Quantitative measurement of IL-1β, IL-6 and TNF-α mRNA in the penumbra area of mice after treatment with different SA formulations. The mice received an intravenous injection one hour after MCAO and were sacrificed 24 h post-injection. Results are showed as mean ± SD, $n = 5$, $^{*}p < 0.05$; $^{**}p < 0.01$. (d)–(f) Super oxide dismutase (SOD), (e) MDA and (f) GSH of normal and MCAO mice treated with different nanoparticles. Data are presented as mean ± SD ($n = 5$); $^{*}p < 0.05$; $^{**}p < 0.01$.

3.8 Biocompatibility of nanoparticles in other organs

It is generally accepted that an ideal nanoparticle should have good biocompatibility without organ toxicity, which makes it important to evaluate the potential toxicity of NPs and T-NPs before their clinical application. From previous experimental results, we found that NPs and T-NPs can accumulate in brain and liver, but they were also distributed in other tissues, including the heart, spleen, lung and kidney. To determine whether NPs and T-NPs cause damage to various organs in mice while treating ischemic stroke, sections of the heart, liver, spleen, kidneys and lungs were frozen. Damage of these organs was not observed by H&E. The myocardial cells in the cardiac tissue were structurally intact and without inflammation in the control group, the MCAO group and the nanoparticle group (Fig. 8). In the liver tissue, the presence of nanoparticles did not affect the function of the liver. In addition, the hepatic lobules were structurally intact and the hepatocytes were arranged neatly (Fig. 8). The structures of the spleen bodies in all the groups were intact and were not affected by the NPs or T-NPs. In the lung, the NPs did not affect the intact structure of the alveoli or thickness of the interstitial wall and the lung function was not affected (Fig. 8). Finally, we examined the effects of NPs on the kidneys and found that the NPs did not change the structure of the renal tubules or renal capsules. In addition, there were no changes in the structure of the kidneys in any of the experimental groups (Fig. 8).

Furthermore, we also tested indicators of liver (Albumin, ALB; Alkaline phosphatase, ALP and Alanine transaminase,

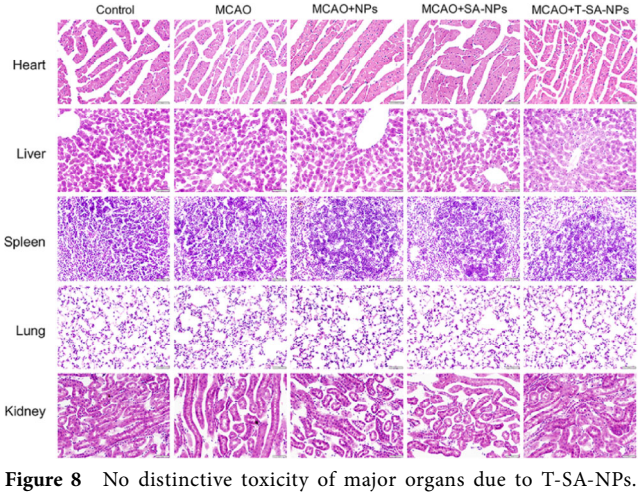

Figure 8 No distinctive toxicity of major organs due to T-SA-NPs. Immunohistochemical staining of liver, lung, kidney, heart and spleen from control, NPs-infused, SA-NPs-infused or T-SA-NPs-infused mice ($n = 5$). No significant pathological changes were observed in the main organs of normal mice after SA-NPs or T-SA-NP tail vein injection.

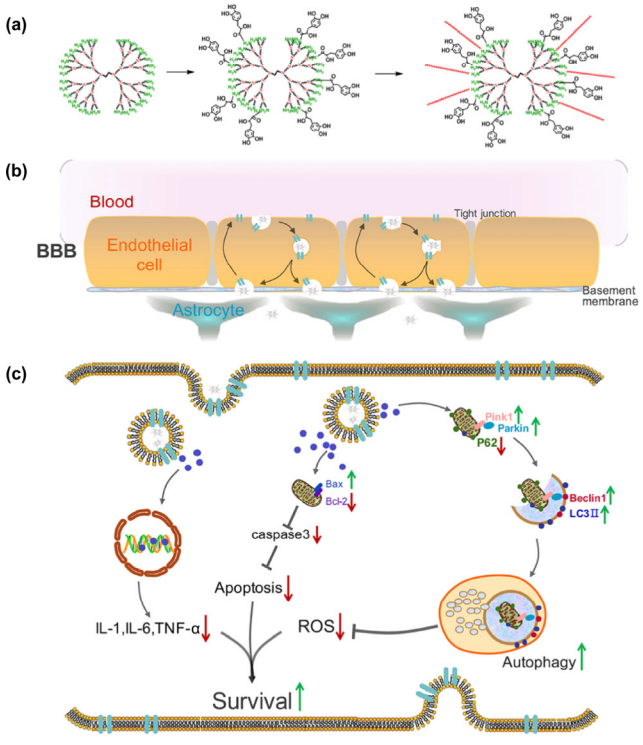

Scheme 1 Scheme of the construction of the T-SA-NPs nanoparticles and the potential mechanism of action. (a) Schematic diagram of the synthesis of the T-SA-NPs nanoparticles. (b) Schematic illustration of the potential mechanism of the penetration of the T-SA-NPs across the BBB. The COG1410 peptide binds cell surface receptors on the brain endothelial cells that form the BBB and mediates the transcytosis of the nanoparticles across the cell layer. (c) Potential mechanism of action of the T-SA-NPs in the damaged neurons cells in ischemic stroke. Internalization of T-SA-NPs allows the relesed SA to protect the cells from the damage of oxidative stress which induced by ischemic stroke.

ALT) and kidney function (blood urea nitrogen, BUN). The results show that the content of ALT increased after ischemic stroke (Fig. S2 in the ESM). However, the content of ALT was significantly decreased after treatment with T-SA-NPs, which might protect the liver from damage experienced during ischemic stroke. In other words, T-SA-NPs treatment played a positive role in protecting the liver. There were no other significant changes in the other indicators of liver function (ALB and ALP) and kidney function (BUN) (Fig. S2 in the ESM), which is consistent with the H&E staining results showing that the nanoparticles are safe in mice.

In addition, the *in vivo* fluorescence assay demonstrated that these nanodrug delivery systems may reach the stroke area and be stored in this area (Fig. 5(a)). Furthermore, the drug could be metabolized in other organs, which indicates the biosafety of nanodrug delivery systems (Fig. 8(a)). Taken together, the *in vivo* results demonstrate the therapic effect of these new nanodrug delivery systems.

4 Conclusion

In this paper, we reported a nanoparticles that are linked to SA and modified with a targeting peptide, COG1410, which can target the lipoprotein receptors of vascular endothelial cells. With these modified nanoparticles, SA was able to pass through the BBB by intracellular endocytosis of ligand-receptor-specific binding. This nanoparticle system was highly efficient in the delivery of SA across the BBB. Here, the delivered SA protected the neurons from ischemic stroke-induced damage in the penumbra area and decreased the neurobehavioral deficits. The mechanism of this protection is potentially mediated by increasing the mitochondrial autophagy flux through Pink1 and Parkin, which reduces inflammation and cell apoptosis. The nanoparticles used in these studies were safe in mice because there were no structural damage and other adverse effects in the brain, heart, spleen, kidney, lung or liver after the treatment with the nanoparticles. Therefore, the prepared nanodrug carrier may be a potential solution for the delivery of SA through the BBB, which is a prospective approach for ischemic stroke therapy.

Conflicts of interest

The authors declare no conflicts of interest. None of the authors has a financial conflict of interest related to this study.

Acknowledgements

This study was supported by the National Natural Science Foundation of China (Nos. 31571020, 31570856 and 21375133), and Beijing Nova Programme Interdisciplinary Cooperation Project (No. Z191100001119002).

Electronic Supplementary Material: Supplementary material (experimentals and results which containing blood-brain barrier permeability *in vitro* and biocompatibility of nanoparticles in other organs) is available in the online version of this article at https://doi.org/10.1007/s12274-020-2930-6.

References

[1] Donnan, G. A.; Fisher, M.; Macleod, M.; Davis, S. M. Stroke. *Lancet* **2008**, *371*, 1612–1623.

[2] Campbell, B. C. V.; Ma, H.; Ringleb, P. A.; Parsons, M. W.; Churilov, L.; Bendszus, M.; Levi, C. R.; Hsu, C.; Kleinig, T. J.; Fatar, M. et al. Extending thrombolysis to 4·5–9 h and wake-up stroke using perfusion imaging: A systematic review and meta-analysis of individual patient data. *Lancet* **2019**, *394*, 139–147.

[3] Coutts, S. B.; Menon, B. K. Late thrombolysis for stroke works, but how do we do it? *Lancet* **2019**, *394*, 97–98.

[4] Chouchani, E. T.; Pell, V. R.; Gaude, E.; Aksentijević, D.; Sundier, S. Y.; Robb, E. L.; Logan, A.; Nadtochiy, S. M.; Ord, E. N. J.; Smith, A. C. et al. Ischemic accumulation of succinate controls reperfusion injury through mitochondrial ROS. *Nature* **2014**, *515*, 431–435.

[5] Yamato, M.; Egashira, T.; Utsumi, H. Application of *in vivo* ESR spectroscopy to measurement of cerebrovascular ROS generation in stroke. *Free Radic. Biol. Med.* **2003**, *35*, 1619–1631.

[6] Kim, C. K.; Kim, T.; Choi, I. Y.; Soh, M.; Kim, D.; Kim, Y. J.; Jang, H.; Yang, H. S.; Kim, J. Y.; Park, H. K. et al. Ceria nanoparticles that can protect against ischemic stroke. *Angew. Chem., Int. Ed. Engl.* **2012**, *51*, 11039–11043.

[7] Parikh, N. S.; Elkind, M. S. V. Divergent effects of lipids on stroke. *Nat. Med.* **2019**, *25*, 543–544.

[8] Liu, X. J.; Yan, L.; Xue, F. Z. The associations of lipids and lipid ratios with stroke: A prospective cohort study. *J. Clin. Hypertens.* **2019**, *21*, 127–135.

[9] Holmes, M. V.; Millwood, I. Y.; Kartsonaki, C.; Hill, M. R.; Bennett, D. A.; Boxall, R.; Guo, Y.; Xu, X.; Bian, Z.; Hu, R. Y. et al. Lipids, lipoproteins, and metabolites and risk of myocardial infarction and stroke. *J. Am. Coll. Cardiol.* **2018**, *71*, 620–632.

[10] Ding, W.; Hudson, L. G.; Liu, K. J. Inorganic arsenic compounds cause oxidative damage to DNA and protein by inducing ROS and RNS generation in human keratinocytes. *Mol. Cell. Biochem.* **2005**, *279*, 105–112.

[11] Liu, L.; Zhang, K.; Sandoval, H.; Yamamoto, S.; Jaiswal, M.; Sanz, E.; Li, Z. H.; Hui, J.; Graham, B. H.; Quintana, A. et al. Glial lipid droplets and ROS induced by mitochondrial defects promote

neurodegeneration. *Cell* **2015**, *160*, 177–190.
[12] Melo, A.; Monteiro, L.; Lima, R. M. F.; De Oliveira, D. M.; De Cerqueira, M. D.; El-Bachá, R. S. Oxidative stress in neurodegenerative diseases: Mechanisms and therapeutic perspectives. *Oxid. Med. Cell. Longev.* **2011**, *2011*, 467180.
[13] Reed, T. T. Lipid peroxidation and neurodegenerative disease. *Free Radic Biol. Med.* **2011**, *51*, 1302–1319.
[14] Rajendran, P.; Nandakumar, N.; Rengarajan, T.; Palaniswami, R.; Gnanadhas, E. N.; Lakshminarasaiah, U.; Gopas, J.; Nishigaki, I. Antioxidants and human diseases. *Clin. Chim. Acta* **2014**, *436*, 332–347.
[15] Fan, Y.; Luo, Q. P.; Wei, J. J.; Lin, R. H.; Lin, L. L.; Li, Y. K.; Chen, Z. R.; Lin, W.; Chen, Q. Mechanism of salvianolic acid B neuroprotection against ischemia/reperfusion induced cerebral injury. *Brain Res.* **2018**, *1679*, 125–133.
[16] Chang, Y.; Hsieh, C. Y.; Peng, Z. A.; Yen, T. L.; Hsiao, G.; Chou, D. S.; Chen, C. M.; Sheu, J. R. Neuroprotective mechanisms of puerarin in middle cerebral artery occlusion-induced brain infarction in rats. *J. Biomed. Sci.* **2009**, *16*, 9.
[17] Yan, R. Y.; Wang, S. J.; Yao, G. T.; Liu, Z. G.; Xiao, N. The protective effect and its mechanism of 3-n-butylphthalide pretreatment on cerebral ischemia reperfusion injury in rats. *Eur. Rev. Med. Pharmacol. Sci.* **2017**, *21*, 5275–5282.
[18] Yang, Y. J.; Su, Y. J.; Wang, D. T.; Chen, Y. H.; Wu, T.; Li, G.; Sun, X. G.; Cui, L. Tanshinol attenuates the deleterious effects of oxidative stress on osteoblastic differentiation via Wnt/FoxO3a signaling. *Oxid. Med. Cell. Longev.* **2013**, *2013*, 351895.
[19] Song, W.; Pu, J.; He, B. Tanshinol protects human umbilical vein endothelial cells against hydrogen peroxide-induced apoptosis. *Mol. Med. Rep.* **2014**, *10*, 2764–2770.
[20] Chong, C. M.; Zhou, Z. Y.; Razmovski-Naumovski, V.; Cui, G. Z.; Zhang, L. Q.; Sa, F.; Hoi, P. M.; Chan, K.; Lee, S. M. Y. Danshensu protects against 6-hydroxydopamine-induced damage of PC12 cells *in vitro* and dopaminergic neurons in zebrafish. *Neurosci. Lett.*, **2013**, *543*, 121–125.
[21] Wei, Y.; Zhang, L.; Yu, Z. P.; Lin, K. S.; Yang, S. F.; Dai, L.; Liu, J. F.; Mao, L. K.; Yuan, F.; Gao, Y. X. Enhanced stability, structural characterization and simulated gastrointestinal digestion of coenzyme Q10 loaded ternary nanoparticles. *Food Hydr.* **2019**, *94*, 333–344.
[22] Liu, C. Z.; Zhang, S. Z.; McClements, D. J.; Wang, D. F.; Xu, Y. Design of Astaxanthin-loaded core-shell nanoparticles consisting of chitosan oligosaccharides and poly (lactic-co-glycolic acid): Enhancement of water solubility, stability, and bioavailability. *J. Agric. Food Chem.* **2019**, *67*, 5113–5121.
[23] Esposito, E.; Drechsler, M.; Puglia, C.; Cortesi, R. New strategies for the delivery of some natural anti-oxidants with therapeutic properties. *Mini-Rev. Med. Chem.* **2019**, *19*, 1030–1039.
[24] Chen, C. T.; Duan, Z. Q.; Yuan, Y.; Li, R. X.; Pang, L.; Liang, J. M.; Xu, X. C.; Wang, J. X. Peptide-22 and cyclic RGD functionalized liposomes for glioma targeting drug delivery overcoming BBB and BBTB. *ACS Appl. Mater. Interfaces* **2017**, *9*, 5864–5873.
[25] Yin, T. T.; Xie, W. J.; Sun, J.; Yang, L. C.; Liu, J. Penetratin peptide-functionalized gold nanostars: Enhanced BBB permeability and NIR photothermal treatment of Alzheimer's disease using ultralow irradiance. *ACS Appl. Mater. Interfaces* **2016**, *8*, 19291–19302.
[26] Yang, J. T.; Kuo, Y. C.; Chen, I. Y.; Rajesh, R.; Lou, Y. I.; Hsu, J. P. Protection against neurodegeneration in the hippocampus using sialic acid- and 5-HT-moduline-conjugated lipopolymer nanoparticles. *ACS Biomater. Sci. Eng.* **2019**, *5*, 1311–1320.
[27] Malvajerd, S. S.; Azadi, A.; Izadi, Z.; Kurd, M.; Dara, T.; Dibaei, M.; Zadeh, M. S.; Javar, H. A.; Hamidi, M. Brain delivery of curcumin using solid lipid nanoparticles and nanostructured lipid carriers: Preparation, optimization, and pharmacokinetic evaluation. *ACS Chem. Neurosci.* **2019**, *10*, 728–739.
[28] Zhang, P.; Omaye, S. T. DNA strand breakage and oxygen tension: Effects of β-carotene, α-tocopherol and ascorbic acid. *Food Chem. Toxicol.* **2001**, *39*, 239–246.
[29] Ekladious, I.; Colson, Y. L.; Grinstaff, M. W. Polymer-drug conjugate therapeutics: Advances, insights and prospects. *Nat. Rev. Drug. Discov.* **2019**, *18*, 273–294.
[30] Mohammed, F.; Ke, W. D.; Mukerabigwi, J. F.; Japir A. A. W. M.; Ibrahim, A.; Wang, Y. H.; Zha, Z. S.; Lu, N. N.; Zhou, M.; Ge, Z. S. ROS-responsive polymeric nanocarriers with photoinduced exposure of cell-penetrating moieties for specific intracellular drug delivery. *ACS Appl. Mater. Interfaces* **2019**, *11*, 31681–31692.
[31] Xiang, J. J.; Liu, X.; Zhou, Z. X.; Zhu, D. C.; Zhou, Q.; Piao, Y.; Jiang, L. M.; Tang, J. B.; Liu, X. R.; Shen, Y. Q. Reactive oxygen species (ROS)-responsive charge-switchable nanocarriers for gene therapy of metastatic cancer. *ACS Appl. Mater. Interfaces* **2018**, *10*, 43352–43362.
[32] Zhang, M.; Song, C. C.; Su, S.; Du, F. S.; Li, Z. C. ROS-activated ratiometric fluorescent polymeric nanoparticles for self-reporting drug delivery. *ACS Appl. Mater. Interfaces* **2018**, *10*, 7798–7810.
[33] Qiao, Y. T.; Wan, J. Q.; Zhou, L. Q.; Ma, W.; Yang, Y. Y.; Luo, W. X.; Yu, Z. Q.; Wang, H. X. Stimuli-responsive nanotherapeutics for precision drug delivery and cancer therapy. *Wires Nanomed. Nanobi.* **2019**, *11*, e1527.
[34] Kalhapure, R. S.; Renukuntla, J. Thermo- and pH dual responsive polymeric micelles and nanoparticles. *Chem. Biol. Int.* **2018**, *295*, 20–37.
[35] Xu, X. D.; Saw, P. E.; Tao, W.; Li, Y. J.; Ji, X. Y.; Bhasin, S.; Liu, Y. L.; Ayyash, D.; Rasmussen, J.; Huo, M. et al. ROS-responsive polyprodrug nanoparticles for triggered drug delivery and effective cancer therapy. *Adv. Mater.* **2017**, *29*, 1700141.
[36] Zhang, X. Q.; Li, L. H.; Li, C. F.; Zheng, H.; Song, H. Y.; Xiong, F. L.; Qiu, T.; Yang, J. Cisplatin-crosslinked glutathione-sensitive micelles loaded with doxorubicin for combination and targeted therapy of tumors. *Carbohydr. Polym.* **2017**, *155*, 407–415.
[37] Sharma, A. K.; Gothwal, A.; Kesharwani, P.; Alsaab, H.; Iyer, A. K.; Gupta, U. Dendrimer nanoarchitectures for cancer diagnosis and anticancer drug delivery. *Drug Dis. Today* **2017**, *22*, 314–326.
[38] Luong, D.; Kesharwani, P.; Deshmukh, R.; Amin, M. C. I. M.; Gupta, U.; Greish, K.; Iyer, A. K. PEGylated PAMAM dendrimers: Enhancing efficacy and mitigating toxicity for effective anticancer drug and gene delivery. *Acta Biomater.* **2016**, *43*, 14–29.
[39] Lu, Y. P.; Han, S. P.; Zheng, H. Y.; Ma, R.; Ping, Y. T.; Zou, J. F.; Tang, H. X.; Zhang, Y. P.; Xu, X. L.; Li, F. Z. A novel RGDyC/PEG co-modified PAMAM dendrimer-loaded arsenic trioxide of glioma targeting delivery system. *Int. J. Nanomedicine* **2018**, *13*, 5937–5952.
[40] Gothwal, A.; Nakhate, K. T.; Alexander, A.; Ajazuddin; Gupta, U. Boosted memory and improved brain bioavailability of rivastigmine: Targeting effort to the brain using covalently tethered lower generation PAMAM dendrimers with lactoferrin. *Mol. Pharmaceutics* **2018**, *15*, 4538–4549.
[41] Sharma, A.; Liaw, K.; Sharma, R.; Zhang, Z.; Kannan, S.; Kannan, R. M. Targeting mitochondrial dysfunction and oxidative stress in activated microglia using dendrimer-based therapeutics. *Theranostics* **2018**, *8*, 5529–5547.
[42] Guo, X. L.; Kang, X. X.; Wang, Y. Q.; Zhang, X. J.; Li, C. J.; Liu, Y.; Du, L. B. Co-delivery of cisplatin and doxorubicin by covalently conjugating with polyamidoamine dendrimer for enhanced synergistic cancer therapy. *Acta Biomater.* **2019**, *84*, 367–377.
[43] Chiou, S. H.; Wu, W. T. Immobilization of *Candida* rugosa lipase on chitosan with activation of the hydroxyl groups. *Biomaterials* **2004**, *25*, 197–204.
[44] Guo, X. L.; Kang, X. X.; Wang, Y. Q.; Zhang, X. J.; Li, C. J.; Liu, Y.; Du, L. B. Co-delivery of cisplatin and doxorubicin by covalently conjugating with polyamidoamine dendrimer for enhanced synergistic cancer therapy. *Acta Biomater.* **2019**, *84*, 367–377.
[45] Jiang, X. C.; Xiang, J. J.; Wu, H. H.; Zhang, T. Y.; Zhang, D. P.; Xu, Q. H.; Huang, X. L.; Kong, X. L.; Sun, J. H.; Hu, Y. L. et al. Neural stem cells transfected with reactive oxygen species-responsive polyplexes for effective treatment of ischemic stroke. *Adv. Mater.* **2019**, *31*, 1807591.
[46] Lu, Y. F.; Li, C.; Chen, Q. J.; Liu, P. X.; Guo, Q.; Zhang, Y.; Chen, X. L.; Zhang, Y. J.; Zhou, W. X.; Liang, D. H. et al. Microthrombus-targeting micelles for neurovascular remodeling and enhanced microcirculatory perfusion in acute ischemic stroke. *Adv. Mater.* **2019**, *31*, 1808361.
[47] Fan, Q.; Chen, M. L.; Fang, X. Y.; Lau, W. B.; Xue, L.; Zhao, L. N.; Zhang, H.; Liang, Y. H.; Bai, X.; Niu, H. Y. et al. Aging might

augment reactive oxygen species (ROS) formation and affect reactive nitrogen species (RNS) level after myocardial ischemia/reperfusion in both humans and rats. *AGE* **2013**, *35*, 1017–1026.

[48] Moloney, J. N.; Cotter, T. G. ROS signalling in the biology of cancer. *Semin. Cell Develop. Biol.* **2018**, *80*, 50–64.

[49] El-Kenawi, A.; Ruffell, B. Inflammation, ROS, and mutagenesis. *Cancer Cell* **2017**, *32*, 727–729.

[50] Manton, K. G.; Volovik, S.; Kulminski, A. ROS effects on neurodegeneration in Alzheimer's disease and related disorders: On environmental stresses of ionizing radiation. *Curr. Alzheimer Res.* **2004**, *1*, 277–293.

[51] Lan, A. P.; Chen, J.; Chai, Z. F.; Hu, Y. The neurotoxicity of iron, copper and cobalt in Parkinson's disease through ROS-mediated mechanisms. *BioMetals* **2016**, *29*, 665–678.

[52] Li, P. Y.; Stetler, R. A.; Leak, R. K.; Shi, Y. J.; Li, Y.; Yu, W. F.; Bennett, M. V. L.; Chen, J. Oxidative stress and DNA damage after cerebral ischemia: Potential therapeutic targets to repair the genome and improve stroke recovery. *Neuropharmacology* **2018**, *134*, 208–217.

[53] Hatefi, Y. ATP synthesis in mitochondria. *Eur. J. Biochem.* **1993**, *218*, 759–767.

[54] Nicholls, D. G. Mitochondrial membrane potential and aging. *Aging Cell* **2004**, *3*, 35–40.

[55] Hüttemann, M.; Lee, I.; Pecinova, A.; Pecina, P.; Przyklenk, K.; Doan, J. W. Regulation of oxidative phosphorylation, the mitochondrial membrane potential, and their role in human disease. *J. Bioenerg. Biomembr.* **2008**, *40*, 445.

[56] Susin, S. A.; Zamzami, N.; Castedo, M.; Daugas, E.; Wang, H. G.; Geley, S.; Fassy, F.; Reed, J. C.; Kroemer, G. The central executioner of apoptosis: Multiple connections between protease activation and mitochondria in Fas/APO-1/CD95- and ceramide-induced apoptosis. *J. Exp. Med.* **1997**, *186*, 25–37.

[57] Kubli, D. A.; Gustafsson, A. B. Mitochondria and mitophagy: The yin and yang of cell death control. *Circ. Res.* **2012**, *111*, 1208–1221.

[58] Kolosowska, N.; Keuters, M. H.; Wojciechowski, S.; Keksa-Goldsteine, V.; Laine, M.; Malm, T.; Goldsteins, G.; Koistinaho, J.; Dhungana, H. Peripheral administration of IL-13 induces anti-inflammatory microglial/macrophage responses and provides neuroprotection in ischemic stroke. *Neurotherapeutics* **2019**, *16*, 1304–1319.

[59] Subramaniam, S. R.; Chesselet, M. F. Mitochondrial dysfunction and oxidative stress in Parkinson's disease. *Prog. Neurobiol.* **2013**, *106–107*, 17–32.

[60] Hauser, D. N.; Hastings, T. G. Mitochondrial dysfunction and oxidative stress in Parkinson's disease and monogenic parkinsonism. *Neurobiol. Dis.* **2013**, *51*, 35–42.

[61] Mondragón-Rodríguez, S.; Perry, G.; Zhu, X. W.; Moreira, P. I.; Acevedo-Aquino, M. C.; Williams, S. Phosphorylation of tau protein as the link between oxidative stress, mitochondrial dysfunction, and connectivity failure: Implications for Alzheimer's disease. *Oxid. Med. Cell. Longev.* **2013**, *2013*, 940603.